

The implementation of a prognostic sea surface skin temperature scheme into climate and weather models

Michael A. Brunke and Xubin Zeng (Institute of Atmospheric Physics, The University of Arizona, Tucson, Arizona)
Vasubandhu Misra (Department of Meteorology, Florida State University, Tallahassee, Florida)
Anton Beljaars (European Centre for Medium-Range Weather Forecasts, Reading, England)

1 Introduction

Numerical weather prediction (NWP) and atmospheric general circulation models (AGCMs) use sea surface temperature (SST) to calculate the surface sensible and latent heat fluxes as the lower boundary condition of the model. Ideally, this should be the actual temperature at the atmosphere-ocean interface, but, generally, it is taken to be the temperature of the uppermost layer in an ocean general circulation model (OGCM) which is typically at a depth of 10 m or that from a pentad- to monthly-averaged SST product such as Reynolds and Smith (1992) blended from satellite and in-situ measurements made at a depth of several cm to a few m.

The difference between the latter temperature, referred to as bulk temperature (T_b), and the actual interfacial temperature or skin temperature (T_s) comes about because of two processes:

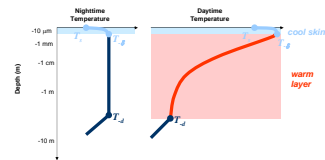


FIGURE 1. A schematic of the ocean temperature of the uppermost ~10 m at nighttime and daytime (based on Donlon et al. 2002). The temperatures T_s , T_a , and T_d are the interfacial or skin, subskin, and depth temperatures referred to in ZB.

•At night and in the day, there is a net cooling within the first few mm, producing a cool skin.

•During the day, a warm layer also forms underneath the cool skin due to the absorption of incoming shortwave radiation.

2 The ZB Scheme

Unlike some recently developed schemes (e.g., Fairall et al. 1996, Clayson and Curry 1996, Gentemann et al. 2003, Zeng et al. 1999), Zeng and Beljaars (2005, hereafter ZB) is a prognostic scheme suitable for modeling in which the temperature differences across the cool skin and warm layer are rigorously derived from the 1-D heat transfer equation:

$$T_s - T_d = \frac{\delta}{\rho_s c_s k_w} (Q + R_s f_s) \quad \text{cool skin}$$

$$\frac{\partial}{\partial t} (T_s - T_d) = \frac{Q + R_s - R(-d)}{\rho_s c_s v(v+1)} - \frac{(v+1)k_w}{d\delta(d/L)} (T_s - T_d) \quad \text{warm layer}$$

The latter assumes that the temperature profile in the warm layer is:

$$T(z) = T_d - \left(\frac{z + \delta}{-d + \delta} \right) (T_s - T_d)$$

where $v = 0.3$ instead of 1 since solar absorption would be greatest near the surface.

Also:

$$\delta = 6 \left\{ 1 + \left[\frac{-16g\alpha v^2}{u_s^2 k_w^2 \rho_s c_s} (Q + R_s f_s) \right]^{1/4} \right\}^{1/2} \quad \text{and } d = 3 \text{ m}$$

$$L = \frac{\rho_s c_s u_s^2}{k_F}$$

$$f_s = \begin{cases} g\alpha_s [Q + R_s - R(-d)] \text{ for } T_s - T_d \leq 0 \\ \frac{g\alpha_s}{(1+g)} \rho_s c_s u_s^2 (T_s - T_d)^2 \text{ for } T_s - T_d > 0 \end{cases}$$

Key to scheme variables

$Q = LH + SH + LW$	$g =$ gravitational acceleration
$R_s =$ surface shortwave radiation	$\alpha_s =$ thermal expansion coefficient
$R(-d) =$ shortwave radiation at d	$\rho_s =$ density of seawater
$f_s =$ fraction of shortwave radiation absorbed in the surface layer	$c_s =$ volumetric heat capacity of seawater
	$k_w =$ molecular thermal conductivity
	$v_s =$ kinematic viscosity of seawater
	$u_s =$ friction velocity in the water
	$k =$ von Karman constant

3 CAM3.1 Runs

Three different versions of CAM3.1 using the Eulerian dynamical core was run at T42 resolution using a climatological annual cycle of SST:

- CONTROL: unaltered version of CAM3.1
- TSKIN: version with ZB implemented.
- RANDOM: version adding a random perturbation uniformly distributed between ±0.1 K.

Each were run for 20 years outputting monthly averages with hourly output for one boreal winter and summer season.

4 Results

The SST diurnal cycle in TSKIN

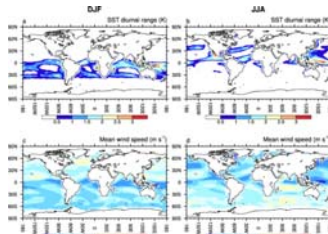


FIGURE 2. The mean diurnal range in sea surface temperature (SST) in TSKIN for December-February (DJF) of Year 4/5 and for June-August (JJA) of Year 5. (c, d) The mean 10-m wind speed in TSKIN for DJF of Year 4/5 and for JJA of Year 5.

•The skin SST diurnal range, i.e., the difference between the maximum and minimum during each day, is < 0.5 K in most oceanic regions but > 0.5 K in mostly tropical and subtropical oceans of the summer hemisphere with > 2 K in isolated areas.

The effect of the SST diurnal cycle on T_a and LH flux

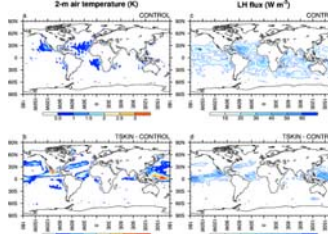


FIGURE 3. (a) The mean diurnal range in 2-m air temperature in JJA of Year 5 for CONTROL and (b) the mean difference between that of TSKIN and CONTROL. (c) The mean diurnal range in surface latent heat flux in JJA of Year 5 for CONTROL and (d) the mean difference between that of TSKIN and CONTROL.

•The mean diurnal cycle in hourly 2-m air temperature and latent heat flux is substantially increased in roughly the same areas where the SST diurnal range is increased.

The effect of the SST diurnal cycle on precipitation

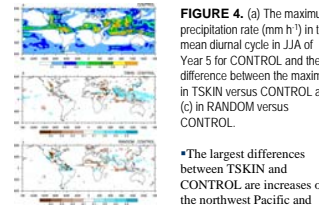


FIGURE 4. (a) The maximum precipitation rate (mm h^{-1}) in the mean diurnal cycle in JJA of Year 5 for CONTROL and the (b) difference between the maximum in TSKIN versus CONTROL and (c) in RANDOM versus CONTROL.

•The largest differences between TSKIN and CONTROL are increases over the northwest Pacific and over the Bay of Bengal, while other differences are spatially incoherent.

•The differences between RANDOM and CONTROL are spatially incoherent over all oceanic regions.

The effect of the SST diurnal cycle on the South Asian monsoon

Miller et al. (1992) showed similar precipitation changes in the ITCZ and over the South Asian monsoon region in JJA.

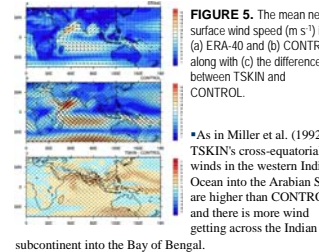


FIGURE 5. The mean near-surface wind speed (m s^{-1}) in (a) ERA-40 and (b) CONTROL along with (c) the difference between TSKIN and CONTROL.

•As in Miller et al. (1992), TSKIN's cross-equatorial winds in the western Indian Ocean into the Arabian Sea are higher than CONTROL, and there is more wind getting across the Indian subcontinent into the Bay of Bengal.

•As in Miller et al. (1992), improved latent heat fluxes (not shown) over the region have led to an enhancement of the large-scale flow, thus resulting in improved monsoon precipitation over the region.

The effect of the SST diurnal cycle on climatological precipitation

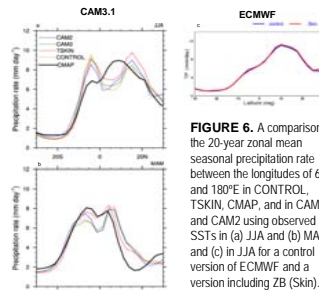


FIGURE 6. A comparison of the 20-year zonal mean seasonal precipitation rate between the longitudes of 60°E and 180°E in CONTROL, TSKIN, CMAP, and in CAM3 and CAM2 using observed SSTs in (a) JJA and (b) MAM, and (c) in JJA for a control version of ECMWF and a version including ZB (Skin).

•ZB is unable to alleviate the major deficiency of producing a double ITCZ in JJA in the region of 60°-180°E. This double ITCZ is not produced in ECMWF.

•The strongest improvement occurs in MAM in which TSKIN increases the precipitation in the fall hemisphere closer to CMAP while leaving the precipitation in the spring hemisphere largely unchanged.

5 Summary and Conclusions

•The implementation of ZB in CAM3.1 has allowed the model to simulate a realistic diurnal cycle in skin SST when using its climatological SST dataset. While the SST diurnal range is generally small (< 0.5 K), it can be > 2 K in isolated areas. Smaller diurnal ranges were obtained when implemented into the ECMWF and an AGCM coupled to an OGCM (Misra et al. 2008), but these models produce stronger tropical winds than in CAM3.1 (not shown).

•While the improved diurnal cycle in SST partially alleviates the model errors in certain regions most notably in seasonal precipitation, it cannot improve the model's major deficiency of producing a double ITCZ in JJA. Further model development may help rectify some of these problems.

•ZB is a cost-effective method to reproduce the diurnal cycle of skin SST without the need to couple to a bulk SST less than once a day. TSKIN runs only 19 seconds more than CONTROL for one year of simulation on a SGI Altix 4700 using 32 nodes.

References

Clayson, C. A., and J. A. Curry, 1996: Determination of surface turbulent fluxes for the Tropical Ocean-Global Atmosphere Response Experiment: Comparison of satellite retrievals and in situ measurements. *J. Geophys. Res.*, **101**, 28 515-28 528.

Donlon, C. J., P. J. Minnett, C. Gentemann, T. J. Nightingale, I. J. Barton, B. Ward, and M. J. Murray, 2002: Toward improved validation of satellite sea surface skin temperature measurements for climate research. *J. Climate*, **15**, 353-369.

Fairall, C. W., E. F. Bradley, J. S. Godfrey, G. A. Wick, and J. B. Edson, 1996: Cool-skin and warm-layer effects on sea surface temperature. *J. Geophys. Res.*, **101**, 1295-1308.

Gentemann, C. L., C. J. Donlon, A. Stuart-Menteth, and F. J. Wentz, 2003: Diurnal signals in satellite sea surface temperature measurements. *Geophys. Res. Lett.*, **30** (3), 1140, doi:10.1029/2002GL016291.

Miller, M. J., A. C. M. Beljaars, and T. N. Palmer, 1992: The sensitivity of the ECMWF model to the parameterization of evaporation from the tropical oceans. *J. Climate*, **5**, 418-434.

Misra, V., L. Marx, M. Brunke, and X. Zeng, 2008: The equatorial Pacific cold tongue bias in a coupled climate model. *J. Climate*, **21**, 5852-5869.

Reynolds, R. W., and T. M. Smith, 1994: Improved global sea surface temperature analyses using optimum interpolation. *J. Climate*, **7**, 929-948.

Zeng, X., and A. Beljaars, 2005: A prognostic scheme of sea surface skin temperature for modeling and data assimilation. *Geophys. Res. Lett.*, **32**, L14605, doi: 10.1029/2005GL023030.

Zeng, X., M. Zhao, R. E. Dickinson, and Y. He, 1999: A multi-year hourly sea surface skin temperature dataset derived from the TOGA TAO bulk temperature and wind speed over the tropical Pacific. *J. Geophys. Res.*, **104**, 1525-1536.

For more information, contact:

Michael A. Brunke
P.O. Box 210081
Tucson, AZ 85721-0081
brunke@atmo.arizona.edu
(520) 626-7439

or read the manuscript:

Brunke, M. A., X. Zeng, V. Misra, and A. Beljaars, 2008: Integration of a prognostic sea surface skin temperature scheme into weather and climate models. *J. Geophys. Res.*, **113**, D21117, doi:10.1029/2008JD010607.